Hydrogenated vacancies and hidden hydrogen in $SrTiO_3$

J. B. Varley
Materials Department, University of California, Santa Barbara, California 93106-5050, USA
and Lawrence Livermore National Laboratory, Livermore, California 94550, USA

A. Janotti and C. G. Van de Walle
Materials Department, University of California, Santa Barbara, California 93106-5050, USA
(Received 1 August 2013; revised manuscript received 21 January 2014; published 4 February 2014)

We investigate the stability of O, Ti, and Sr vacancies in $SrTiO_3$ and their interactions with hydrogen impurities. Based on density functional calculations with a hybrid functional, we analyze formation energies, binding energies, and H-related vibrational modes. We find that interstitial hydrogen (H_i^+) and substitutional hydrogen on an oxygen site (H_O) both act as shallow donors and are likely to contribute to unintentional n-type conductivity. Hydrogen can also bind to Ti vacancies in the form of $(V_{Ti}\text{-H})^{-3}$ and $(V_{Ti}\text{-2H})^{-2}$ complexes. Sr vacancies can form $(V_{Sr}\text{-H})^-$ or accommodate an H_2 molecule in the form of $(V_{Sr}\text{-}H_2)^{-2}$ complex. The latter provides an explanation for the "hidden" hydrogen recently observed in annealing experiments [M. C. Tarun and M. D. McCluskey, J. Appl. Phys. **109**, 063706 (2011)].

DOI: 10.1103/PhysRevB.89.075202 PACS number(s): 61.72.Bb, 63.20.Pw, 61.72.J−, 71.55.Ht

I. INTRODUCTION

Strontium titanate ($SrTiO_3$ or STO) is a key material in the development of oxide-based electronic devices [1,2]. It often serves as a substrate for ferroelectrics and high-T_c superconductors [2]. More recently, STO has been shown to hold a two-dimensional electron gas (2DEG) at the interface with other complex oxides such as $LaAlO_3$ [3] or $GdTiO_3$ [4], focusing attention on the use of STO as a semiconductor in its own right. As in any semiconductor, the electronic properties of STO can be strongly affected by the presence of native defects and impurities. Native point defects in STO have been recently studied using first-principles calculations [5–7], and the role of the hydrogen impurity has been investigated both experimentally [8–10] and theoretically [11,12]. Experiments indicate that H impurities can be readily incorporated into STO. Klauer and Wöhlecke resolved the configuration of H incorporated as an interstitial (H_i) [9] using polarized Raman scattering. Recent infrared (IR) spectroscopy measurements by Tarun and McCluskey indicate the existence of an H-related defect that is stable up to temperatures of 1100 °C [10]. It was proposed that hydrogen impurities form complexes with Sr vacancies (V_{Sr}) and give rise to local vibrational modes in the range of 3350–3600 cm^{-1}. The experiments also revealed that some of the hydrogen exists in a form that cannot be detected using IR spectroscopy. This "hidden" hydrogen is released as H_i^+ upon annealing at temperatures ∼400–500 °C [10]. Calculations based on density functional theory (DFT) in the local density approximation (LDA) have been performed to identify the H-related vibration frequencies [12], yet the source of hidden hydrogen has remained elusive.

Here we perform a comprehensive investigation of hydrogen in STO and its interaction with native defects. We use first-principles calculations based on DFT, employing a hybrid functional that overcomes the band-gap problem associated with the use of conventional functionals such as the LDA or generalized gradient approximation (GGA). We find that H acts as a shallow donor when incorporating in interstitial sites (H_i^+) or substitutionally on the O site (H_O^+). We also find that H interacts strongly with the cation vacancies, forming stable complexes with Ti vacancies (V_{Ti}) and Sr vacancies (V_{Sr}). We describe these defects in terms of their formation energies and binding energies with respect to H_i^+.

Our results shown that H can enhance n-type conductivity in STO in two distinct ways. First, by increasing the free carrier concentration as a shallow donor, and second, by passivating native defects that act as compensating centers, specifically by lowering the charge state of highly charged cation vacancies. We discuss the vibrational frequencies associated with these defects, providing an identification for the modes observed in recent experiments [10]; the signals 3350–3390 cm^{-1} are most likely related to O-H stretch modes of a complex composed of two interstitial H and a Ti vacancy $[(V_{Ti}\text{-H})^{-2}]$. Finally, we explored complexes involving interstitial H_2 molecules that possibly behave as hydrogen reservoirs. We find that only the Sr vacancy can accommodate an H_2 molecule in a stable manner, explaining the release of interstitial H_i^+ at temperatures ∼400–500 °C [10] and providing an unambiguous explanation for the source of hidden hydrogen in STO.

II. DETAILS OF THE CALCULATIONS

The calculations are based on generalized Kohn-Sham formalism with the HSE06 screened hybrid functional [13] and the projector augmented-wave method, as implemented in the VASP code [14–17]. The Hartree-Fock mixing parameter is set to 25%, resulting in values for band gap [18], lattice constant [19], and enthalpy of formation [20] of cubic STO that are in good agreement with experiments (Table I) and previous calculations using hybrid functionals [6,7,21]. The Ti semicore 3s and 3p electrons were treated as core electrons, as tests show that their inclusion leads to changes in formation energies of less than 0.1 eV. For the defect calculations we use a 135-atom supercell, a 2 × 2 × 2 Monkhorst-Pack k-point sampling, and a plane-wave basis set with a cutoff of 400 eV. Corrections due to finite-size effects resulting from the long-range Coulomb interaction of charged defects in a homogeneous neutralizing

TABLE I. Calculated structural parameters, indirect (R-Γ) and direct (Γ-Γ) band gaps, and formation enthalpies for cubic STO. Structural parameters and formation enthalpies of TiO_2, SrO, and H_2O are also listed. Experimental values from taken from Refs. [18–20].

Material	Property	Theory	Experiment
$SrTiO_3$	a (Å)	3.905	3.900
	E_g^i(R-Γ) (eV)	3.11	3.25
	E_g^d(Γ-Γ) (eV)	3.41	3.75
	ΔH_f (eV)	− 16.22	− 17.13
TiO_2	a (Å)	4.617	4.593
	c (Å)	2.953	2.958
	ΔH_f (eV)	− 9.07	− 9.11
SrO	a (Å)	5.156	5.140
	ΔH_f (eV)	− 5.60	− 6.14
H_2O	H-O (Å)	0.961	0.958
	H-O-H (deg)	105.2	104.5
	ΔH_f (eV)	− 2.51	− 2.62

background were explicitly included following the scheme of Freysoldt *et al*. [22,23]. Due to the very large static dielectric constant of STO ($\epsilon_0 = 370$ at room temperature) [24], the effects of the finite-size corrections are dominated by the term describing the proper alignment of the electrostatic potentials of the bulk and defect-containing supercells.

Formation energies are key quantities from which we can derive impurity and defect concentrations, stability of different charge states, and the related charge-state transition levels [25]. As an example, the formation energy of V_{Sr} is given by

$$E^f\left(V_{Sr}^q\right) = E_{tot}\left(V_{Sr}^q\right) - E_{tot}(\text{STO}) + \mu_{Sr} + q \cdot \epsilon_F + \Delta^q, \quad (1)$$

where $E_{tot}(V_{Sr}^q)$ is the total energy of the supercell containing a vacancy in charge state q, and E_{tot}(STO) is that of a perfect crystal in the same supercell. The chemical potential μ_{Sr}, referenced to the total energy per atom of bulk Sr, can in principle vary over a wide range given by the stability condition of $SrTiO_3$:

$$\mu_{Sr} + \mu_{Ti} + 3\mu_O = \Delta H_f(SrTiO_3), \quad (2)$$

with $\mu_{Sr} \leqslant 0$, $\mu_{Ti} \leqslant 0$, and $\mu_O \leqslant 0$. The chemical potential μ_{Ti} is referenced to the energy per atom of Ti bulk, and μ_O to half the energy of molecular O_2. μ_{Sr}, μ_{Ti}, and μ_O are further constrained by the formation of TiO_2 and SrO:

$$\mu_{Ti} + 2\mu_O < \Delta H_f(TiO_2), \quad (3)$$

$$\mu_{Sr} + \mu_O < \Delta H_f(SrO). \quad (4)$$

For a given value of μ_O, μ_{Ti} and μ_{Sr} can therefore vary over a range:

$$\Delta H_f(SrTiO_3) - \Delta H_f(SrO) - 2\mu_O < \mu_{Ti} < \Delta H_f(TiO_2) - 2\mu_O, \quad (5)$$

$$\Delta H_f(SrTiO_3) - \Delta H_f(TiO_2) - \mu_O < \mu_{Sr} < \Delta H_f(SrO) - \mu_O. \quad (6)$$

For the defects containing hydrogen we reference the chemical potential μ_H to half of the total energy of an H_2 molecule. In the O-rich limit μ_H is limited by the formation of H_2O, i.e.,

$$2\mu_H + \mu_O < \Delta H_f(H_2O). \quad (7)$$

The term $q \cdot \epsilon_F$ in Eq. (1) represents the electron chemical potential or Fermi level ϵ_F, i.e., the energy of the reservoir with which electrons are exchanged to form the charged defect. We reference ϵ_F to the valence-band maximum (VBM), and plot formation energies as a function of ϵ_F ranging from the VBM to the conduction-band minimum (CBM). Since STO is almost always n type, we focus our analysis of formation energies and binding energies on ϵ_F at the CBM ($=E_g$). Finally, the last term in Eq. (1) is the charge-state dependent correction due to the finite size of the supercell [22,23].

III. RESULTS AND DISCUSSION

The calculated lattice constant, band gap, and formation enthalpy of STO are listed in Table I. We also list the calculated structural parameters and formation enthalpy of TiO_2, SrO, and H_2O. The formation enthalpies are used to establish bounds for the chemical potentials that determine the defect formation energies, according to Eqs. (2)–(7). The calculated values of all quantities listed in Table I are in good agreement with experiment.

Figure 1 shows the range of μ_{Ti} and μ_O values for which STO is stable. The chemical potential μ_O can, in principle, vary over a very wide range from 0 to −5.60 eV, while μ_{Ti} can vary from 0 to −10.62 eV, as long as Eq. (1) is satisfied. For increasing μ_O and μ_{Ti}, the stability of STO is limited by the formation of TiO_2, whereas in the low μ_O and μ_{Ti} region, the stability of STO is limited by the formation of SrO.

In the following discussion we present the results for (i) $\mu_O = 0$ (points A and B in Fig. 1), corresponding to

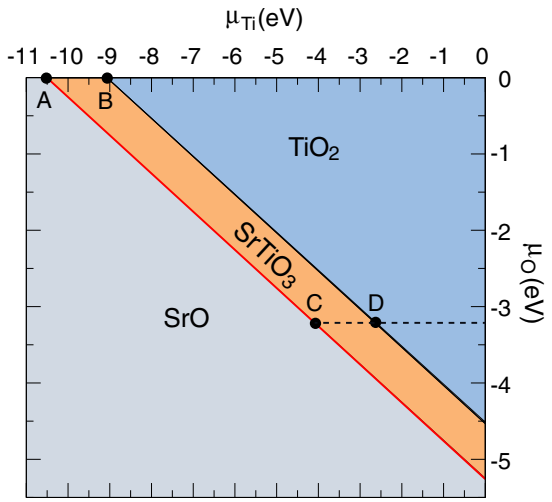

FIG. 1. (Color online) Allowed values of Ti and O chemical potentials defining the stability of $SrTiO_3$. The chemical potentials μ_O, μ_{Ti}, and μ_{Sr} are limited by the formation of the SrO and TiO_2 as described in the text. The line joining A and B corresponds to $\mu_O = 0$, while the line between C and D corresponds to $\mu_O = -3.20$ eV, i.e., to the experimental conditions in Ref. [10] (see text).

TABLE II. Formation energies of point defects, impurities, and complexes in STO, in all calculated charge states. Chemical potentials are set to the elemental reference energies, and the Fermi level is chosen at the VBM. Values associated with an asterisk (∗) indicate the defect is not stable as a localized charge state, i.e., that the conduction (valence) band was populated with the electron (hole) rather than the defect.

Defect	+2	+1	0	−1	−2	−3	−4
H_2	–	–	2.60	–	–	–	–
H_i	–	−2.00	1.59	5.55	–	–	–
V_O	−1.31	*	*	–	–	–	–
H_O	–	0.89	*	–	–	–	–
V_O-H_2	−0.59	*	*	–	–	–	–
V_{Ti}	–	–	16.11	16.69	17.46	18.14	18.92
V_{Ti}-H	–	–	13.04	13.60	14.31	14.92	*
V_{Ti}-2H	–	–	10.20	10.84	11.47	*	*
V_{Ti}-H_2	–	–	–	–	–	18.76	21.00
V_{Sr}	–	–	*	*	10.52	–	–
V_{Sr}-H	–	–	*	7.50	*	–	–
V_{Sr}-2H	–	–	4.81	*	*	–	–
V_{Sr}-H_2	–	–	*	*	10.78	–	–

oxygen-rich conditions—in this case $\mu_H = \Delta H_f(H_2O)/2 = -1.26$ eV; and (ii) $\mu_O = -3.20$ eV and $\mu_H = -0.61$ eV (points C and D), corresponding to the hydrogenation conditions in the experiments of Tarun and McCluskey [10,26]. In the hydrogenation experiments, the STO single crystal is placed in a quartz ampoule that is filled with 1/2 atm H_2 gas and then heated to 800 °C. This value of $\mu_O = -3.20$ eV also corresponds to that set in annealing experiments on STO single crystals using mixtures of O_2 with air, Ar, or Ar/H_2, with O_2 partial pressure varying from 10^{-13} to 10^{-14} Pa at 800 °C [27].

A summary of the calculated formation energies for all defects, impurities, and complexes considered in the present work is presented in Table II. Individual cases will be discussed in the following subsections.

A. Interstitial hydrogen and interstitial H_2 molecules

The most stable configuration of an isolated H interstitial is shown in Fig. 2(a). We find H located in the (001) plane, bonded to an O atom, with an H–O bond length of 0.98 Å, and forming an H-O-Ti angle of 76°. These results are similar to those reported in Ref. [12]. Interstitial H is stable exclusively in the positive charge state. Therefore, it acts as a shallow donor and may contribute to n-type conductivity in STO. This behavior is similar to that found in other wide-band-gap oxide materials [28–33], and is related to the low position of the conduction-band edge on an absolute energy scale [34].

We also considered the possibility of placing an H_2 molecule at interstitial sites. The lowest energy configuration is for H_2 in the (001) plane, oriented along the [110] direction, as shown in Fig. 2(b); the equilibrium H–H bond length is 0.73 Å, very close to the value for an H_2 molecule in free space (0.74 Å). Interstitial H_2 is electrically inactive, i.e., it is stable exclusively in the neutral charge state. The occupied bonding state is 7 eV below the VBM and the empty antibonding state is resonant in the conduction band.

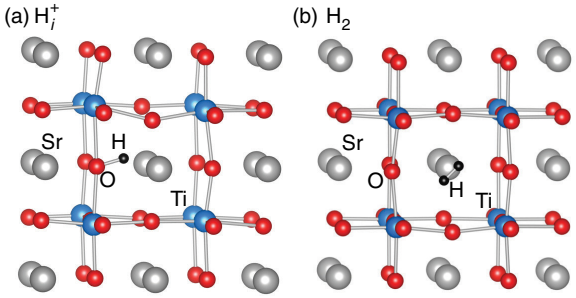

FIG. 2. (Color online) Lowest energy configurations for (a) interstitial hydrogen H_i^+ and (b) an interstitial hydrogen molecule (H_2) in STO. The interstitial H atom bonds to an O atom in the (001) plane, forming an H-O-Ti angle of 76°. The interstitial H_2 molecule sits in a (001), within a TiO_2 plane, with the H–H bond oriented along the [110] direction.

Figure 3 shows the formation energy as a function of Fermi level for interstitial H and H_2, for $\mu_O = 0$ (corresponding to points A and B in Fig. 1), and $\mu_O = -3.20$ eV (corresponding to points C and D). For $\mu_O = 0$ we take $\mu_H = -1.26$ eV, corresponding to equilibrium with H_2O, and for points C and D we take $\mu_H = -0.61$ eV corresponding to the free energy of H_2 gas at 800 °C and 1/2 atm (hydrogenation conditions in Ref. [10]). The formation energy of H_i^+ increases linearly with the Fermi level; H_i^+ has moderate formation energy in n-type STO. Interstitial H_2 has a much higher formation energy than H_i^+ and is thus very unlikely to incorporate.

B. Oxygen vacancies and H on the oxygen site (H_O)

Removing an O atom from the STO lattice leaves two Ti dangling bonds to be occupied by two electrons. These dangling bonds combine into a bonding state in the gap and an antibonding state resonant in the conduction band. In the case of a vacancy in the neutral charge state (V_O^0), the state in the gap is occupied by two electrons, with opposite spins; for V_O^+, the state in the gap is singly occupied. We find that V_O^0 and V_O^+ are always higher in energy than V_O^{+2}. In the +2 charge

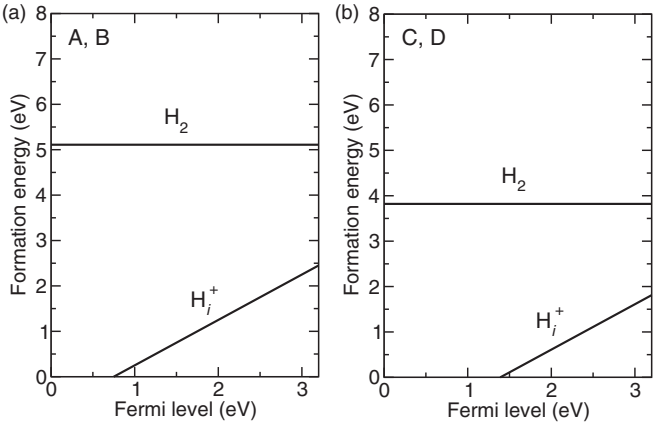

FIG. 3. Formation energy of interstitial H (H_i^+) and interstitial H_2 molecule in STO. The chemical potentials are set to (a) $\mu_O = 0$, $\mu_H = -1.26$ eV, corresponding to points A and B in Fig. 1, and (b) $\mu_O = -3.20$ eV, $\mu_H = -0.61$ eV, corresponding to points C and D.

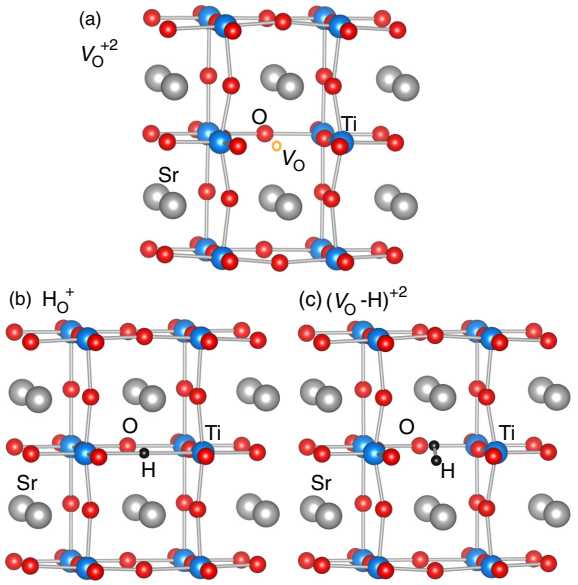

FIG. 4. (Color online) Local lattice configurations for (a) the doubly ionized oxygen vacancy (V_O^{+2}), (b) the substitutional H (H_O^+), and (c) the H_2 molecule occupying an oxygen site [$(V_O\text{-}H_2)^{+2}$].

state, the neighboring Ti atoms are displaced away from the vacant site by as much as 0.11 Å [Fig. 4(a)], lifting the bonding state that was in the gap for the neutral charge state to become resonant in the conduction band.

An O vacant site can be occupied by an H atom. We find that the H atom, instead of moving off site toward one of the Ti neighbors, prefers to sit on site, equally bonding to the two Ti neighbors as shown in Fig. 4(b), with an H–Ti bond length of 2.02 Å (to be compared with the equilibrium O–Ti bond length of 1.95 Å). In this three-center-bond configuration, the substitutional H_O^+ acts as a shallow donor, similar to the behavior in other wide-gap oxides such as ZnO [35], SnO_2 [31], TiO_2 [33], and $BaTiO_3$ [36].

In principle, an H_2 molecule can also sit at the O vacant site, as shown in Fig. 4(c). The H–H bond is perpendicular to the axis connecting the two Ti neighbors, and oriented along the [110] direction. This complex is most stable in the +2 charge state $(V_O\text{-}H_2)^{+2}$, being composed of a doubly ionized vacancy V_O^{+2} and a neutral H_2 molecule. This interpretation is based on the facts that (a) the Ti-Ti distance in the complex 4.19 Å is slightly larger than the Ti-Ti distance in the isolated V_O^{+2}, (b) the H-H distance of 0.76 Å is very close to that in the isolated interstitial H_2, and (c) no gap states are present.

The formation energies as a function of Fermi level for V_O^{+2}, H_O^+, and $(V_O\text{-}H_2)^{+2}$ are shown in Fig. 5. The binding energy of H_O^+ with respect to dissociation into V_O^{+2} and H_i^+, calculated as $E_b = E^f(V_O^{+2}) + E^f(H_i^+) - E^f(H_O{}^+)$ is 2.3 eV for ϵ_F at the CBM; combined with the calculated value for the migration barrier of H_i^+ of 0.25 eV [12], we estimate that H_O^+ is stable up to 500 °C [37]. As V_O^{+2} would repel the positively charged H_i^+ present in the lattice, we expect H_O^+ to form only during growth, annealing, or in hydrogenation experiments. Finally, we observe that the complex $(V_O\text{-}H_2)^{+2}$ is energetically highly unfavorable.

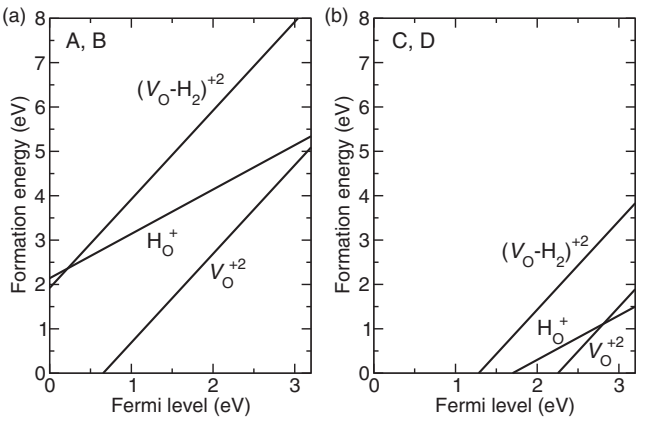

FIG. 5. Formation energies of the doubly ionized vacancy (V_O^{+2}), substitutional H (H_O^+), and an H_2 molecule sitting on the O site [$(V_O\text{-}H_2)^{+2}$] for (a) O-rich conditions ($\mu_O = 0$, A and B points in Fig. 1), and (b) $\mu_O = -3.20$ eV (C and D points in Fig. 1), corresponding to the conditions in the experiments of Ref. [10].

C. Titanium vacancies and complexes with hydrogen

The Ti atoms in STO are sixfold coordinated, sitting at the center of TiO_6 octahedra. Thus, the removal of a Ti atom leaves six O dangling bonds, with a total of four missing electrons (holes). In *n*-type STO, the Ti vacancy is most stable in the −4 charge state V_{Ti}^{-4}, and all six O atoms are displaced slightly away from the vacancy by 0.14 Å, resulting in O-O distances of 2.95 Å along the [110] and 4.17 Å along the [100] directions [Fig. 6(a)]. These O-O distances are too large to allow the formation of O–O bonds.

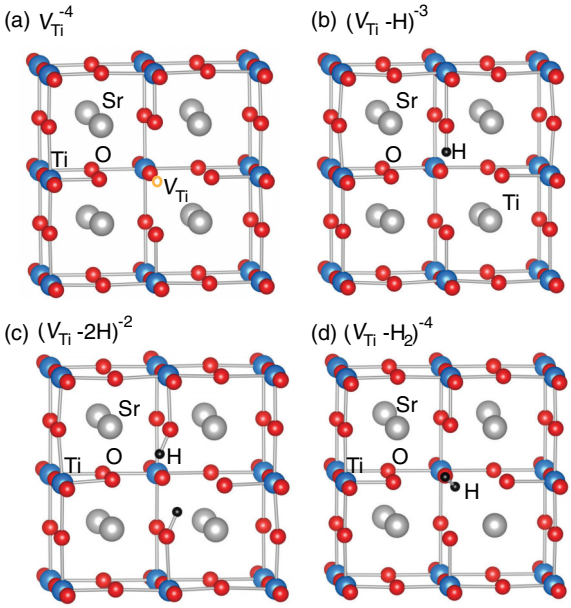

FIG. 6. (Color online) Local lattice configurations for (a) a Ti vacancy in the −4 charge state (V_{Ti}^{-4}), (b) one H atom bonded to an O atom in the Ti vacancy [$(V_{Ti}\text{-H})^{-3}$], (c) two H atoms bonded to O atoms in the Ti vacancy [$(V_{Ti}\text{-2H})^{-2}$], and (d) an H_2 molecule in the Ti vacancy [$(V_{Ti}\text{-}H_2)^{-4}$].

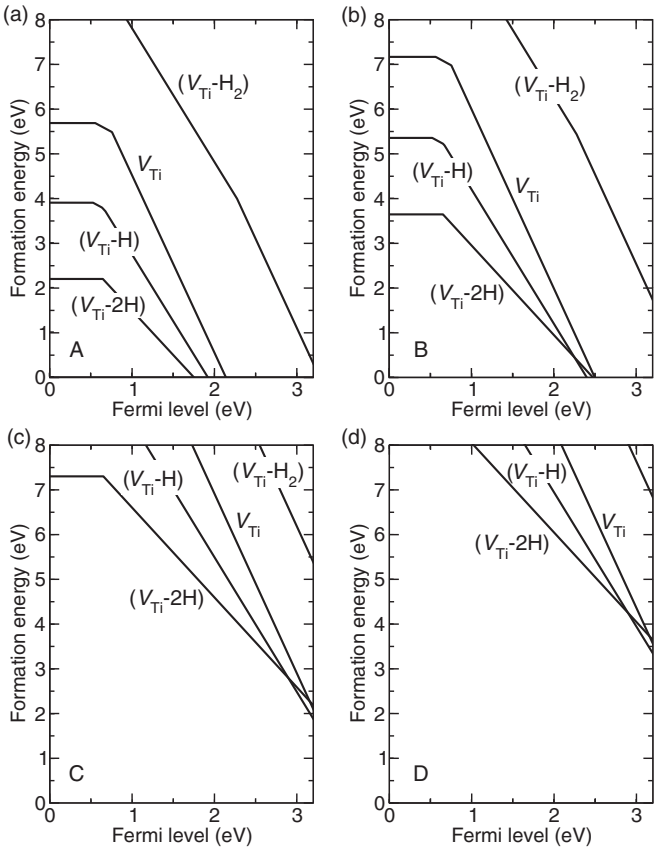

FIG. 7. Formation energies of the Ti vacancy (V_{Ti}), one H atom bonded to an O atom in the Ti vacancy [(V_{Ti}-H)], two H atoms bonded to O atoms in the Ti vacancy [(V_{Ti}-2H)], and an H_2 molecule in the Ti vacancy [(V_{Ti}-H_2)], for different sets of chemical potentials (A, B, C, and D, see Fig. 1).

Since the Ti vacancy is negatively charged in n-type STO, and since it contains O dangling bonds, we expect it to form complexes with positively charged interstitial H. Indeed, we find that V_{Ti} can accommodate one or two H atoms. The complex with one H atom is stable in the -3 charge state $(V_{Ti}\text{-H})^{-3}$, and the complex with two H is stable in the -2 charge state $(V_{Ti}\text{-2H})^{-2}$, the atomic configurations of which are shown in Figs. 6(b) and 6(c). In the case of $(V_{Ti}\text{-H})^{-3}$, the O–H bond length is 0.98 Å with the bond oriented along the [001] direction. In the case of $(V_{Ti}\text{-2H})^{-2}$ the two H atoms are bonded to O atoms that are on opposite side of the vacancy, as shown in Fig. 6(c) with a bond length of 0.97 Å. The O-H bonds deviate from the [001] direction by an angle of 21° due to Coulomb repulsion, resulting in an H–H distance of 2.22 Å.

We also explored the possibility of placing an H_2 molecule at the Ti vacancy. Since this complex consists of a V_{Ti}^{-4} and a neutral H_2 molecule, it is stable in the -4 charge state in n-type STO, $(V_{Ti}\text{-}H_2)^{-4}$. The H–H bond, with a length of 0.72 Å, is oriented along the [111] direction with the center of mass at the original Ti site, as shown in Fig. 6(d), and an O-O distance along the [100] direction of 4.27 Å, compared to 4.18 Å for the isolated V_{Ti}^{-4}. The shortest distance between H and O in this complex is 1.95 Å, indicating an absence of O–H bonding.

Figure 7 shows the formation energies of the Ti vacancy and its complexes with hydrogen. Conditions A and B, both for $\mu_O = 0$, correspond to different μ_{Ti} values, as shown in Fig. 1, and similarly for C and D. For the latter, V_{Ti}^{-4}, $(V_{Ti}\text{-H})^{-3}$, and $(V_{Ti}\text{-2H})^{-2}$ have similar formation energies for ϵ_F at the CBM. The binding energy of $(V_{Ti}\text{-H})^{-3}$ with respect to dissociation into V_{Ti}^{-4} and H_i^+ is 2.0 eV. In the case of $(V_{Ti}\text{-2H})^{-2}$, the binding energy with respect to $(V_{Ti}\text{-H})^{-3}$ and H_i^+ is 1.5 eV. Combined with the migration barrier of H_i^+, we estimate [37] that $(V_{Ti}\text{-2H})^{-2}$ is stable up to 350 °C, and $(V_{Ti}\text{-H})^{-3}$ up to 450 °C.

A hydrogen molecule trapped in an V_{Ti}^{-4} vacancy $(V_{Ti}\text{-}H_2)^{-4}$ constitutes a local minimum in the potential energy landscape, i.e., a metastable state distinct from $(V_{Ti}\text{-2H})^{-2}$ described above. However, it is much higher in energy than $(V_{Ti}\text{-2H})^{-2}$, for all Fermi level values in the band gap (Fig. 7). It is thus very unlikely that the trapped-molecule configuration would form, which is to be expected given that the Ti vacancy is surrounded by O dangling bonds that are very reactive to H atoms.

D. Strontium vacancies and complexes with hydrogen

The Sr atoms are surrounded by 12 nearest-neighbor oxygen atoms with Sr-O distances of 2.76 Å. The Sr atoms contribute two electrons to the valence bands derived from the covalent bonds between the Ti and O atoms. In this view, the Sr atoms are ionically bonded to a network of TiO_6 octahedra. Removing a Sr atom therefore leaves two holes in the valence band. In n-type material, the Sr vacancy is stable in the -2 charge state (V_{Sr}^{-2}), causing negligible disturbance in the STO lattice, as shown in Fig. 8(a).

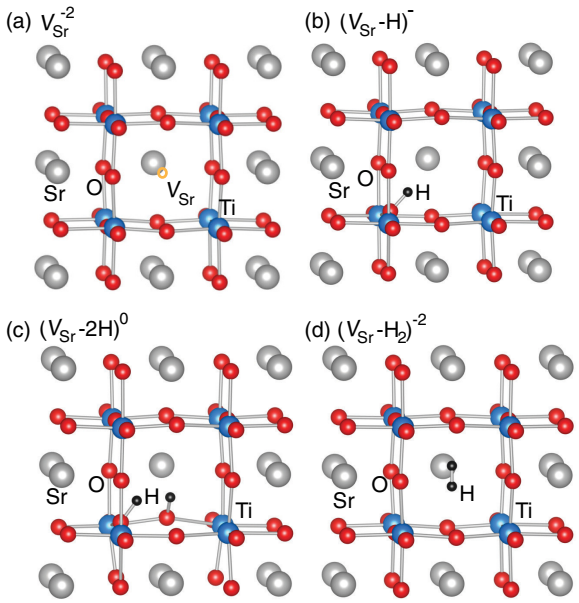

FIG. 8. (Color online) Local lattice configurations for (a) a Sr vacancy in the -2 charge state (V_{Sr}^{-2}), (b) one H atom bonded to an O atom in the Sr vacancy [$(V_{Sr}\text{-H})^{-}$], (c) two H atoms bonded to O atoms in the Sr vacancy [$(V_{Sr}\text{-2H})^{0}$], and (d) an H_2 molecule in the Sr vacancy [$(V_{Sr}\text{-}H_2)^{-2}$].

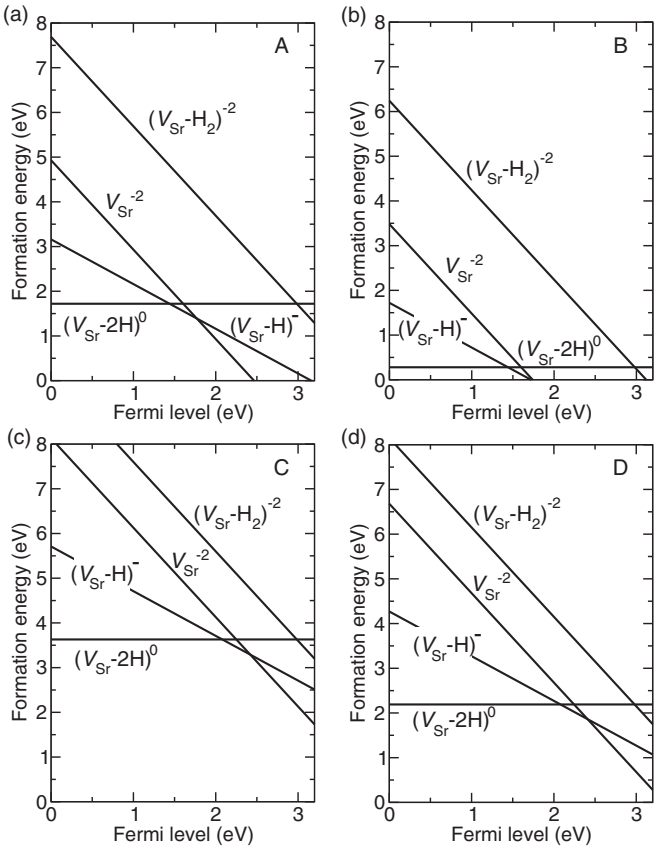

FIG. 9. Formation energies of the negatively charged Sr vacancy (V_{Sr}^{-2}), one H atom bonded to an O atom in the Sr vacancy [$(V_{Sr}\text{-H})^-$], two H atoms bonded to O atoms in the Sr vacancy [$(V_{Sr}\text{-2H})^0$], and an H_2 molecule in the Sr vacancy [$(V_{Sr}\text{-}H_2)^{-2}$], for different sets of chemical potentials (A, B, C, and D, see Fig. 1).

Being negatively charged, it is expected that V_{Sr}^{-2} can form complexes with H_i^+. Indeed we find that V_{Sr}^{-2} can bind up to two H atoms, resulting in negatively charged $(V_{Sr}\text{-H})^-$ and neutral $(V_{Sr}\text{-2H})^0$. In the case of $(V_{Sr}\text{-H})^-$, the H atom is bonded to one of the O atoms neighboring the vacancy, with an O–H bond length of 0.97 Å, oriented toward the vacancy along the [110] direction, and with the O-H unit pulled slightly toward the vacancy [Fig. 8(b)]. In the case of $(V_{Sr}\text{-2H})^0$, the second H atom can bond to any of the other 11 O atoms neighboring the vacancy, with formation energies differing by less than 0.2 eV, in agreement with the results in Ref. [12]. Figure 8(c) shows a configuration in which the H atoms are bonded to two O atoms that are in the same plane and close to each other. The Sr vacancy can also accommodate an H_2 molecule, the resulting complex being stable in the -2 charge state $(V_{Sr}\text{-}H_2)^{-2}$. The H–H distance is 0.74 Å and the bond is oriented along the [001] direction as shown in Fig. 8(d).

The formation energies of the Sr vacancy and related complexes are shown in Fig. 9. In n-type STO, the isolated V_{Sr}^{-2} is lower in energy than the hydrogenated vacancy. Still, the binding energy of $(V_{Sr}\text{-H})^-$ with respect to the dissociation into V_{Sr}^{-2} and H_i^+ is 1.0 eV, and that of $(V_{Sr}\text{-2H})^0$ with respect to $(V_{Sr}\text{-H})^-$ and H_i^+ is 0.7 eV. Adding the migration barrier of H_i^+, the estimated temperature for dissociation of $(V_{Sr}\text{-2H})^0$ and $(V_{Sr}\text{-H})^-$ is 150 °C.

We also find that an H_2 molecule trapped in a Sr vacancy $(V_{Sr}\text{-}H_2)^{-2}$ has lower formation energy than $(V_{Sr}\text{-2H})^0$ in n-type material. This is in contrast to what happens in the Ti vacancy, where the H atoms prefer to form O–H bonds. Indeed, in the V_{Sr}^{-2} no covalent bonds are broken and thus there is no strong incentive for H to bond to O. When two H atoms are introduced into the vacancy, they prefer to bond to each other, leading to an H_2 molecule trapped in the vacancy, a configuration that is more stable than $(V_{Sr}\text{-2H})^0$, at least under n-type conditions. This has important consequences for the type of H-related vibrational frequencies that are observed, and for the source of hidden hydrogen, as discussed in the next section.

TABLE III. Theoretical and experimental values for the frequencies of hydrogen-related vibrational modes, in cm^{-1}. ω_1, ω_2, and ω_3 are measured frequencies from Ref. [10]. The calculated values ω^c include a systematic correction of 53 cm^{-1}, as described in the text, to allow a more direct comparison with experiment.

Type	Configuration	$d_{O\text{-}H}$ (Å)	ω (Expt.)	ω_c (Theory)
ω_1	H_I	–	3500	
ω_2	H_{II}	–	3355	
ω_3	H_{II}	–	3384	
H_i^+	Interstitial	0.964		3500
$(V_{Sr}\text{-H})^{-1}$	–	0.967		3679
$(V_{Sr}\text{-2H})^0$	H_a	0.967		3679
	H_b	0.967		3687
$(V_{Ti}\text{-H})^{-3}$	–	0.975		3545
$(V_{Ti}\text{-2H})^{-2}$	H_a	0.975		3323
	H_b	0.975		3364

E. Hydrogen-related vibrational frequencies and hidden hydrogen

To aid in the identification of the H-related complexes, we calculated the stretch-mode vibrational frequencies of the O–H bonds. The procedure involves introducing small displacements of the H atom along the direction of the bond, toward and away from the O atom. The change in total energy versus distance results in a potential-energy curve, from which we determine the frequency, using the O-H reduced mass of 0.9481 amu. Anharmonic effects are included [38] (Table III). Vibrational frequencies calculated in this fashion can still have an error bar of up to 100 cm^{-1}; however, a large part of this error is systematic and can be attributed to the fact that hybrid functionals tend to overestimate vibrational frequencies by a few percent [39]. We therefore included an additional correction, based on the difference in the calculated and experimental frequencies for the hydrogen interstitial H_i^+ (referred to as the H_I signal in the experimental literature [8–10]). We find a correction of 53 cm^{-1}, which is then applied to the calculated frequencies (all of which involve similar O–H bonds), resulting in the ω^c values in Table III.

Infrared spectroscopy [8–10] reveals signals at ∼3500 cm^{-1} (H_I) that were assigned to interstitial H. Our calculated stretch frequency for H_i^+, listed in Table III,

agrees with this assignment. Recent measurements [10] show the existence of two additional signals in the 3350–3390 cm^{-1} range (H_{II}) that are correlated to each other. These peaks were assigned to two H bonded to a Sr vacancy [10], as in the complex shown in Fig. 8(c). However, our calculated frequencies for $(V_{Sr}\text{-H})^{-}$ and $(V_{Sr}\text{-2H})^{0}$ are far too high to account for the H_{II} signals. No peaks in the range of 3670–3690 cm^{-1}, as calculated for $(V_{Sr}\text{-2H})^{0}$, were observed in the observed IR spectra, consistent with our conclusion that this complex prefers to form $(V_{Sr}\text{-}H_2)^{-2}$, i.e., an H_2 molecule trapped in the Sr vacancy, which would be invisible to the IR measurement.

Turning to V_{Ti}-related complexes, our calculated frequencies for $(V_{Ti}\text{-2H})^{-2}$, as well as their difference, nicely match the H_{II} signals. Thus, based on the calculated vibrational frequencies and calculated stability, we propose that $(V_{Ti}\text{-2H})^{-2}$ is the source of the H_{II} signals.

We now comment on the comparison of our present results with previous calculations. Our conclusion that $(V_{Ti}\text{-2H})^{-2}$ is the source of the H_{II} signals is in agreement with the conclusion in Ref. [40]. With regard to V_{Sr}, the authors of Ref. [12] also concluded that $(V_{Sr}\text{-2H})^{0}$ complexes are not responsible for the H_{II} signals. However, in contrast to the present study, those authors found much lower frequencies for the H-related modes of $(V_{Sr}\text{-2H})^{0}$, around 3500 cm^{-1}, and suggested them to be the origin of the H_I peak. As to interstitial hydrogen, their calculated frequency [12] for H_i^+ was 2745 cm^{-1}, reinforcing their belief that interstitial H could not be responsible for the H_I peak. This calculated frequency of 2745 cm^{-1} is much lower than our calculated value. We attribute this difference mainly to the use of the LDA for the calculations performed in Ref. [12], which tends to severely overestimate the interaction between H and next-nearest neighbor O atoms.

Finally, we address the source of hidden hydrogen in the experiments of Ref. [10]. Tarun and McCluskey suggested that a reservoir of IR-inactive hidden hydrogen exists in STO, which starts to release hydrogen at temperatures above 400 °C. Our results suggest two possible microscopic origins for the "hidden" hydrogen: (i) an H_2 molecule in the Sr vacancy $[(V_{Sr}\text{-}H_2)^{-2}]$, as shown in Fig. 8(d), and (ii) substitutional hydrogen (H_O^+), as shown in Fig. 4(b). In (i), the H_2 signal would be invisible in IR measurements because of the lack of a dipole moment in H_2. The stability of this complex also explains why O-H vibrational modes associated with $(V_{Sr}\text{-2H})^{0}$ are not observed, since this complex is unstable with respect to the formation of $(V_{Sr}\text{-}H_2)^{-2}$. In (ii), the frequency of H_O^+ falls in the region where *n*-type STO is opaque due to free-carrier absorption, and therefore difficult to detect using IR measurements. Other possible sources of hidden hydrogen, such as interstitial H_2 or H_2 trapped in V_O^{+2} or V_{Ti}^{-4} can be ruled out because they are either too high in energy or unstable.

IV. SUMMARY

In summary, we have presented first-principles results for structure and energetics of vacancies and complexes with hydrogen impurities in STO. We find that H_i^+ and H_O^+ are both shallow donors. H_i^+ explains the observed IR signals at ~3500 cm^{-1}, while H_O^+ is possibly a source of hidden hydrogen. The complex of a Ti vacancy with two H atoms $(V_{Ti}\text{-2H})^{-2}$ explains the vibrational frequencies of 3350–3390 cm^{-1} observed for the H_{II} signal [10]. The complex $(V_{Sr}\text{-2H})^{0}$ is unstable with respect to the formation of an H_2 molecule in the Sr vacancy, which can act as a source of IR-inactive hidden hydrogen.

ACKNOWLEDGMENTS

Discussions with B. Jalan and M. D. McCluskey are gratefully acknowledged. This work was supported by the U.S. Army Research Office (W911-NF-11-1-0232) and by the NSF MRSEC Program (DMR-1121053). Computing resources were provided by the Center for Scientific Computing from the CNSI/MRL under NSF MRSEC (DMR-1121053) and NSF (CNS-0960316), and XSEDE (DMR-070072N) which is supported by NSF (OCI-1053575). Part of this work was performed under the auspices of the U.S. Department of Energy at Lawrence Livermore National Laboratory under Contract DE-AC52-07A27344.

[1] T. Yajima, Y. Hikita, and H. Y. Hwang, Nat. Mater. **10**, 198 (2011).
[2] R. Ramesh and D. G. Schlom, MRS Bull. **33**, 1006 (2008).
[3] A. Ohtomo and H. Y. Hwang, Nature (London) **427**, 423 (2004).
[4] P. Moetakef, T. A. Cain, D. G. Ouellette, J. Y. Zhang, D. O. Klenov, A. Janotti, C. G. Van de Walle, S. Rajan, S. J. Allen, and S. Stemmer, Appl. Phys. Lett. **99**, 232116 (2011).
[5] T. Tanaka, K. Matsunaga, Y. Ikuhara, and T. Yamamoto, Phys. Rev. B **68**, 205213 (2003).
[6] M. Choi, F. Oba, and I. Tanaka, Phys. Rev. Lett. **103**, 185502 (2009).
[7] F. El-Mellouhi, E. N. Brothers, M. J. Lucero, and G. E. Scuseria, J. Phys.: Condens. Matter **25**, 135501 (2013).
[8] G. Weber, S. Kapphan, and M. Wöhlecke, Phys. Rev. B **34**, 8406 (1986).
[9] S. Klauer and M. Wöhlecke, Phys. Rev. Lett. **68**, 3212 (1992).
[10] M. C. Tarun and M. D. McCluskey, J. Appl. Phys. **109**, 063706 (2011).
[11] L. Villamagua, R. Barreto, L. M. Procel, and A. Stashans, Phys. Scr. **75**, 374 (2007).
[12] J. T-Thienprasert, I. Fongkaew, D. J. Singh, M.-H. Du, and S. Limpijumnong, Phys. Rev. B **85**, 125205 (2012).
[13] J. Heyd, G. E. Scuseria, and M. Ernzerhof, J. Chem. Phys. **118**, 8207 (2003); **124**, 219906 (2006).
[14] G. Kresse and J. Furthmüller, Phys. Rev. B **54**, 11169 (1996).
[15] G. Kresse and D. Joubert, Phys. Rev. B **59**, 1758 (1999).
[16] P. E. Blöchl, Phys. Rev. B **50**, 17953 (1994).
[17] M. Marsman, J. Paier, A. Stroppa, and G. Kresse, J. Phys.: Condens. Matter **20**, 064201 (2008).
[18] K. van Benthem, C. Elsasser, and R. H. French, J. Appl. Phys. **90**, 6156 (2001).
[19] L. Cao, E. Sozontov, and J. Zegenhagen, Phys. Status Solidi (a) **181**, 387 (2000).

[20] K. Jacob and G. Rajitha, J. Chem. Thermodyn. **43**, 51 (2011).
[21] F. El-Mellouhi, E. N. Brothers, M. J. Lucero, and G. E. Scuseria, Phys. Rev. B **84**, 115122 (2011).
[22] C. Freysoldt, J. Neugebauer, and C. G. Van de Walle, Phys. Rev. Lett. **102**, 016402 (2009).
[23] C. Freysoldt, J. Neugebauer, and C. G. Van de Walle, Phys. Status Solidi (b) **248**, 1067 (2011).
[24] H. Weaver, J. Phys. Chem. Solids **11**, 274 (1959).
[25] C. G. Van de Walle and J. Neugebauer, J. Appl. Phys. **95**, 3851 (2004).
[26] M. W. Chase Jr., *NIST-JANAF Themochemical Tables*, 4th ed., J. Phys. Chem. Ref. Data (NIST, Washington, DC, 1998), Monograph 9, 1-1951.
[27] K. Kerman, C. Ko, and S. Ramanathan, Phys. Chem. Chem. Phys. **14**, 11953 (2012).
[28] C. G. Van de Walle, Phys. Rev. Lett. **85**, 1012 (2000).
[29] C. Kiliç and A. Zunger, Phys. Rev. Lett. **88**, 095501 (2002).
[30] J. Robertson and P. Peacock, Thin Solid Films **445**, 155 (2003).
[31] A. K. Singh, A. Janotti, M. Scheffler, and C. G. Van de Walle, Phys. Rev. Lett. **101**, 055502 (2008).
[32] S. Limpijumnong, P. Reunchan, A. Janotti, and C. G. Van de Walle, Phys. Rev. B **80**, 193202 (2009).
[33] J. B. Varley, A. Janotti, and C. G. Van de Walle, Adv. Mater. **23**, 2343 (2011).
[34] C. G. Vande Walle and J. Neugebauer, Nature (London) **423**, 626 (2003).
[35] A. Janotti, C. G. Van de Walle, Nat. Mater. **6**, 44 (2007).
[36] Y. Kobayashi, O. J. Hernandez, T. Sakaguchi, T. Yajima, T. Roisnel, Y. Tsujimoto, M. Morita, Y. Noda, Y. Mogami, A. Kitada, M. Ohkura, S. Hosokawa, Z. Li, K. Hayashi, Y. Kusano, J. Kim, N. Tsuji, A. Fujiwara, Y. Matsushita, K. Yoshimura, K. Takegoshi, M. Inoue, M. Takano, and H. Kageyama, Nat. Mater. **11**, 507 (2012).
[37] Estimation based on a hopping rate $\Gamma = \Gamma_0 \exp(-E_a/kT)$ of one per minute, and $\Gamma_0 = 100$ THz.
[38] S. Limpijumnong, J. E. Northrup, and C. G. Van de Walle, Phys. Rev. B **68**, 075206 (2003).
[39] A. P. Scott and L. Radom, J. Phys. Chem. **100**, 16502 (1996).
[40] I. Fongkaew, J. T-Thienprasert, D. Singh, M.-H. Du, and S. Limpijumnong, Ceram. Int. **39**, S273 (2013).